European Journal of Applied Physiology
https://doi.org/10.1007/s00421-023-05303-3

ORIGINAL ARTICLE

Kinematics and mechanical changes with step frequency at different running speeds

R. M. Mesquita[1] · P. A. Willems[1] · G. Catavitello[1] · A. H. Dewolf[1]

Received: 24 January 2023 / Accepted: 22 August 2023

Abstract

Purpose Running at a given speed can be achieved by taking large steps at a low frequency or on the contrary by taking small steps at a high frequency. The consequences of a change in step frequency, at a fixed speed, affects the stiffness of the lower limb differently. In this study, we compared the running mechanics and kinematics at different imposed step frequencies (from 2 step s^{-1} to 3.6 step s^{-1}) to understand the relationship between kinematic and kinetic parameters.

Methods Eight recreational male runners ran on a treadmill at 5 different speeds and 5 different step frequencies. The lower-limb segment motion and the ground reaction forces were recorded. Mechanical powers, general gait parameters, lower-limb movements and coordination were investigated.

Results At low step frequencies, in order to limit the magnitude of the ground reaction force, the vertical stiffness is reduced and thus runners deviate from an elastic rebound. At high step frequencies, the stiffness is increased and the elastic rebound is optimised in its ability to absorb and restore energy during the contact phase.

Conclusion We studied the consequences of a change in step frequency on the bouncing mechanics of running. We showed that the lower limb stiffness and the intersegmental coordination of the lower-limb segments are affected by running step frequency rather than speed. The runner rather adapts their lower limb stiffness to match a step frequency for a given speed than the opposite.

Keywords Bouncing mechanism · Intersegmental coordination · Stiffness · Neuromechanics

List of symbols

BW	Body weight
CoM	Centre of mass
GRF	Ground reaction force
F_x, F_y, F_z	Lateral, fore aft and vertical components of the GRF
a_f, a_v and v_f, v_v	Fore-aft (f) and vertical (v) accelerations and velocities of the CoM
E_{com}, E_{kf}, E_v	Energy of the CoM, kinetic energy about the fore-aft direction, vertical energy
E^i_{int}	Internal energy of each segment (i) in relation to the CoM
k_{vert}	Vertical stiffness of the CoM spring
PV	Percentage of variance
ROM	Range of motion
$S_{c,down}$ and $S_{c,up}$	S_v During the contact phases divided into its down and upwards increment
SF, SFs and PSF	Step frequency, step frequencies and preferred step frequencies
SL, L_{ce}, L_{ae}	Step length, effective contact and effective aerial lengths
S_v	Vertical displacement of the CoM
T, t_c and t_a	Step, contact and aerial times
t_{brake} and t_{push}	Time spent braking and spent re-accelerating the CoM during t_c
t_{ce} and t_{ae}	Effective contact time and effective aerial time
u_{3t}, u_{3s}, u_{3f}	Direction cosines of the thigh, shank and foot of the normal covariation plane
v_{belt} and V_{avg}	Speed of the treadmill belt and average of v_{belt} over one stride
W^+_{ext}	Positive external work of the CoM

Communicated by Jean Rene Lacour.

✉ A. H. Dewolf
dewolf.art@gmail.com

[1] Laboratory of Biomechanics and Physiology of Locomotion, Institute of NeuroScience, Université Catholique de Louvain, Place P. de Coubertin, 1, 1348 Louvain-la-Neuve, Belgium

Published online: 08 September 2023

$\dot{W}^{+}_{ext}$ and $\dot{W}^{+}_{ext,push}$	Positive external power of the CoM over a step and over t_{push}
W^{+}_{int} and $\dot{W}^{+}_{int}$	Positive internal work and power of the segments as compared to the CoM

Introduction

Running is a cyclic movement that alternates between unipodal contact and aerial phases. During these phases, the centre of mass (CoM) of the body exhibits a motion comparable to a mass m (equivalent to the body mass) attached to a weightless spring, rebounding off the ground (Blickhan 1989) and oscillating around an equilibrium point where the vertical force equals the body weight (BW). Consequently, the vertical oscillation of the CoM is divided into two parts (Cavagna et al. 1988). First, an effective contact period (t_{ce}), occurring during the contact phase, and representing the lower part of the oscillation during which the vertical ground reaction force (GRF) is greater than body weight. Second, an effective aerial period (t_{ae}), taking place both during the contact and aerial phases, representing the upper part of the oscillation during which the GRF is smaller than body weight.

In this model, the supporting leg behaves like a spring with a 'dual action' stance phase: throughout the first part of contact, the spring-mass system is compressed and potential elastic energy is stored into the muscle–tendon units of the lower limb to be further released during the second part of contact when the spring expands. During t_{ce}, the half period of the elastic oscillation, a linear relationship between the vertical component of GRF (F_z) and the vertical displacement (S_v) of the CoM exists. Therefore, the stiffness (k_{vert}) of the spring-mass model, reflecting the overall limb behaviour, can be approximated by the slope of the F_z-S_v relation. When humans increase their step frequency at a given running speed, the most important adjustment to the body's spring system is that the spring becomes stiffer (Dewolf et al. 2022; Farley and González 1996).

Running at a given speed can be achieved by taking large steps at a low frequency or on the contrary by taking small steps at a high frequency. The choice of the preferred step frequency (PSF) has been carefully documented by Cavagna et al. (1988, 1991). However, what are the consequences of a change in step frequency, and in turn of spring stiffness, on the running kinematic and kinetic parameters?

First, from a mechanical point of view, because the spring-mass system oscillates around a point of equilibrium at which $F_z = BW$, the vertical momentum lost and gained during t_{ce} must equal the vertical momentum lost and gained during t_{ae}. When running at speeds up to ~3.1 m s^{-1}, t_{ce} approximates t_{ae} (symmetric step). As speed increases above 3.1 m s^{-1}, t_{ae} is greater than t_{ce} and the step becomes asymmetric (Cavagna et al. 1988; Dewolf et al. 2016; Schepens et al. 1998). Decreasing the step frequency (SF) below the PSF requires an increase in step length (L) to maintain the same constant speed. Indeed, an 'unusually' long step at a low frequency requires a decreased vertical stiffness (Farley and González 1996). During the contact phase, the distance travelled by the CoM is limited due to anatomical restrictions (Cavagna et al. 1988), thus an asymmetric rebound would be observed at lower step frequencies. In addition, a longer aerial phase demands greater external power generated during the contact phase to accelerate and lift the CoM appropriately. Thus, one could expect to observe adjustments to the bouncing mechanism similar to those observed when running on a slope (Dewolf et al. 2016) or against a hindering traction force (Mesquita et al. 2020) to limit the increase in muscular power. At frequencies higher than PSF, the vertical stiffness increases (Farley and González 1996), which potentially implies that the bounce remains symmetric as speeds increase, in this way the muscular power done to move the CoM should no longer be a limiting factor.

Second, from a kinematic point of view, the lower limb intersegmental coordination during stance is expected to contribute to the modification of stiffness. Indeed, the body is a dynamical system where the position in space of the CoM depends among others on the overall configuration of the lower limb segments. In particular, the vertical displacement of the CoM and the stiffness of the lower limb depends on the configuration of the lower limb segments, the thigh, shank, and foot, during the stance phase.

Movements of the lower-limb segments and their coordination can be investigated using the planar covariation method (Bianchi et al. 1998; Borghese et al. 1996). These studies have shown that the changes of the angular motion of the lower-limb segments covary along a plane indicating a reduction in the degrees of freedom of the system from three to two. The planar covariation law shows that a general kinematic coordination pattern is maintained in various animal species (Catavitello et al. 2018; Courtine et al. 2005; Ogihara et al. 2014), in different locomotor conditions (Borghese et al. 1996; Catavitello et al. 2015; Dewolf et al. 2018; Grasso et al. 2000), and is adapted with the speed of progression (Ivanenko et al. 2007). However, to the best of our knowledge, the relationship between stiffness and the intersegmental coordination has never been explored.

Although the modification of step frequency and running has been extensively studied (Cavagna et al. 1988, 1991; Farley and González 1996; Lieberman et al. 2015; McMahon and Cheng 1990; van Oeveren et al. 2021), the relationship between the bouncing mechanism and the kinematic coordination of the lower limb segments when modifying step frequency still raises many interesting unanswered questions. The aim of this paper is to shed light on the

consequences of a change in step frequency on the running mechanics. Five different imposed step frequencies and the preferred step frequency (PSF) were analysed at four different running speeds to try to answer this question. When running at higher SFs, we expect the bouncing mechanics to remain symmetrical, whereas the more the runner decreases their SF below the PSF the more their bouncing mechanics becomes asymmetrical for a similar speed. The kinematic synergy of the lower limb segments has been shown to adapt with speed (Ivanenko et al. 2007), however, a change in SF either increases/decreases the range of motion of the lower limbs and thus of their segments. Consequentially, this could change the relationship between them and, as seen in (Barliya et al. 2009), change the coordination patterns. The aim of this study was to investigate how changes in step frequency affect movement patterns and to better understand how the body's dynamic system adapts its leg configuration, and, therefore, its spring stiffness, to perform these more complex movements.

Methods

Participants and experimental procedure

Eight recreational healthy male runners with no injuries in the last 6 months participated in the study. The number of subjects chosen was based on an a priori statistical power analysis from results of a pilot study (Mesquita et al. 2021). The anthropometric and running characteristics of the subjects are presented in Table 1. Informed written consent was obtained and the study followed the guidelines of the Declaration of Helsinki. All procedures were accepted by the UCLouvain ethical committee (B403201838331).

Participants ran on a treadmill at four different constant speeds: 8, 11, 14 and 17 km h^{-1} (corresponding to 2.22, 3.06, 3.89 and 4.72 m s^{-1}, respectively). At each speed, subjects were asked to run at 6 different step frequencies: their preferred step frequency (PSF), and 2.0, 2.4, 2.8, 3.2, 3.6 step s^{-1} conveyed via an electronic metronome and amplified on loudspeakers. This range of SFs was chosen based on Cavagna et al. (1991) where the authors showed that such frequencies correspond to the range where subjects are able to run at all speeds. To remove the effect of learning and fatigue and secure statistical independency, the different speeds and frequencies were presented randomly. A one-hour training session was done at least two days prior to recordings. At the end of the training session all subjects were able to run within ± 5% of the imposed frequency.

The instruction given during the trials was that each foot strike should correspond to a beat of the metronome. For each trial, the treadmill belt accelerated until the target speed was reached. After an auditory check by the experimenters ensuring that the subject was running approximately at the correct SF, the recording began and lasted 10 s. The belt then decelerated, and in total each trial lasted ≈ around 1 min.

After each recording, a check of the average SF over the entire trial was done with a custom written algorithm (Matlab, Mathworks, 2019 Natick, Massachusetts, USA) that used the *fft* routine on the vertical ground reaction force waveform. If the computed SF did not match the required one ± 6% of error, the participant was asked to repeat the trial.

Experimental setup

Participants ran on an instrumented treadmill (h/p/Cosmos, Germany—Arsalis, Belgium) with a belt surface of 1.6 × 0.65 m. The entire treadmill was mounted onto four strain-gauge force transducers that measure the three components of the GRF exerted by the treadmill under the foot (Willems and Gosseye 2013). Each transducer's analogue

Table 1 Participants' anthropometric information and each subject's PSF at the different speeds along with the averages and standard deviations for each class

Subject	Subject information				Preferred step frequency (steps s^{-1})			
	Height (m)	Mass (kg)	Leg length (m)	Age (years)	08 km h^{-1}	11 km h^{-1}	14 km h^{-1}	17 km h^{-1}
1	1.88	74.1	0.98	21	2.44	2.44	2.62	2.74
2	1.83	68.7	0.96	21	2.75	2.70	2.74	2.84
3	1.83	70.4	0.95	22	2.40	2.58	2.53	2.66
4	1.82	68.0	0.92	22	2.76	2.90	2.92	2.95
5	1.89	83.9	0.99	23	2.76	2.85	3.01	3.10
6	1.79	69.4	0.91	24	2.77	2.89	2.93	3.00
7	1.87	77.2	1.00	22	2.56	2.61	2.68	2.74
8	1.80	78.2	0.97	23	2.65	2.79	3.01	3.15
Mean	1.84	73.7	0.96	22.2	2.66	2.72	2.81	2.90
SD	0.03	5.65	3.19	1.03	0.14	0.17	0.18	0.18

signals were amplified, low-pass filtered (4-pole Bessel filter with a -3 dB cut-off frequency at 200 Hz) to avoid an aliasing effect during digitisation and recorded with a sampling rate of 1 kHz. After digitalisation, the force signals were filtered by a two-way 8th order Bessel filter with a lowpass cut-off frequency at 10 Hz for the lateral F_x, 20 Hz for fore-aft F_y and 30 Hz for vertical F_z forces (Mesquita et al. 2020).

The electrical motor of the belt was also instrumented with an optical angle encoder to measure the speed of the belt (v_{belt}). When the participants ran on the treadmill, the recorded average speed of the belt over a stride (V_{avg}) differed by $2.8 \pm 1.4\%$ from the chosen speed and the instantaneous v_{belt} did not change by more than 5% of V_{avg}.

Bilateral, full-body three-dimensional (3D) kinematics was recorded at 200 Hz by means of a Qualisys system with thirteen cameras (12 Mocap OQUS 6 + cameras and 1 video MIQUS M1 camera, Qualisys, Sweden) placed around the treadmill. Participants were equipped with 29 retro-reflective markers glued onto the skin at the following positions: chin-neck intersect (Neck), sternum (Chest), superior surface of acromion (Shoulder), lateral epicondyle of humerus (Elbow), ulnar styloid process (Wrist), superior anterior iliac spine (Waist), superior posterior iliac spine (BackWaist), greater trochanter (GT), mid-thigh (Thigh), external condyle of femur (Knee), shin (Shank), lateral malleolus (Ankle), heel (Heel), fifth metatarsophalangeal joint (VM) and second metatarsophalangeal joint (IIM) on both sides of the body. Kinematic data were then oversampled at 1 kHz using the spline routine in Matlab. An oversampling of the kinematic data was chosen rather than a down sampling of the kinetic data to ensure that the force signal characteristics were not lost during data-processing. The kinematic data were filtered by the same filter with a lowpass cut-off frequency at 30 Hz.

Data processing

Data processing was performed via custom made programs written with LABVIEW (National Instruments 2019, Austin, Texas, USA) and Matlab software.

Assessment of general gait parameters

Figure 1 illustrates the time curves of the vertical and fore-aft components of the GRF in two of the four speed classes and all frequency classes. A stride period is defined based from the foot contacts. A foot contact corresponds to the moment at which the vertical component of the ground reaction force (F_z) becomes greater than ten percent of BW. The stride period is defined as the time between a right foot contact and the next right foot contact and the step period is defined as the time between the foot contact of one leg until and the next foot contact of the contralateral leg. The effective contact time, t_{ce}, corresponds to the period during which $F_z \geq$ BW and the effective aerial time, t_{ae}, corresponds to the period during which $F_z <$ BW as in Cavagna et al. (2009). Furthermore, the contact phase (t_c), the period between the touch-down and take-off of the corresponding foot, can also be divided into an initial braking phase (t_{brake}) followed by a pushing phase (t_{push}). t_{brake} is defined as the time spent decelerating the CoM during t_c and t_{push} as the time spent re-accelerating it preceding the take-off phase.

We considered valid strides when: (1) the average vertical force during the stride ($\overline{F_z}$) is within 5% of BW, (2) the sum of the increments and the sum of the decrements of the instantaneous velocity (v_y) of the CoM differed less than 25% as in Dewolf et al. (2016), (3) the step frequency was equal to the metronome step frequency $\pm 5\%$. In total 2385 valid strides (4790 steps, 599 ± 75 steps per subject, mean $\pm$ SD) were selected.

Computation of acceleration, velocity and vertical displacement of the CoM

The acceleration, velocity and displacement of the CoM was calculated from the GRF as in Gosseye et al. (2010) and in Mesquita et al. (2020). Briefly, the fore-aft and vertical CoM accelerations were obtained, respectively, as $a_f = \frac{F_y}{m}$ and $a_v = \frac{F_z}{m} - g$. We did not consider the lateral component of the GRF since its contribution is negligible (Willems et al. 1995).

A time-integration of the a_f, and a_v-recordings give the fore-aft (v_f) and vertical (v_v) velocity changes of the CoM. Integrations are performed numerically by the trapezoidal method. An integration constant must be added to v_f, and v_v to obtain the components of the instantaneous velocities of the CoM relative to a reference frame fixed to the treadmill as in Gosseye et al. (2010). The vertical (S_v) displacement of the CoM relative to the treadmill is then computed by numerical integration of v_v. S_v can be further divided during the contact phase into two periods: after touchdown while the CoM is descending until its minimum ($S_{c,down}$) and then once the CoM is rising until take-off ($S_{c,up}$).

Computation of the external work (E_{com}), work (W_{ext}) and push-averaged power ($\dot{W}_{ext}$)

The energy of the CoM (E_{com}) done in respect to its environment was computed based on the fore-aft and vertical movements of the CoM. The energy due to the fore-aft movements of the CoM (E_{kf}) can be computed by: $E_{kf} = \int F_y(v_f - V_{avg})dt = \frac{1}{2}m(v_f - V_{avg})^2$, where V_{avg} is the average speed of the treadmill. The energy of the CoM due to its vertical movements (E_v) can be computed by: $E_v = \int (F_z v_v)\, dt = \frac{1}{2}mv_v^2 + mgS_v$. Then, the E_{com} is given by $E_{com} = E_{kf} + E_v$.

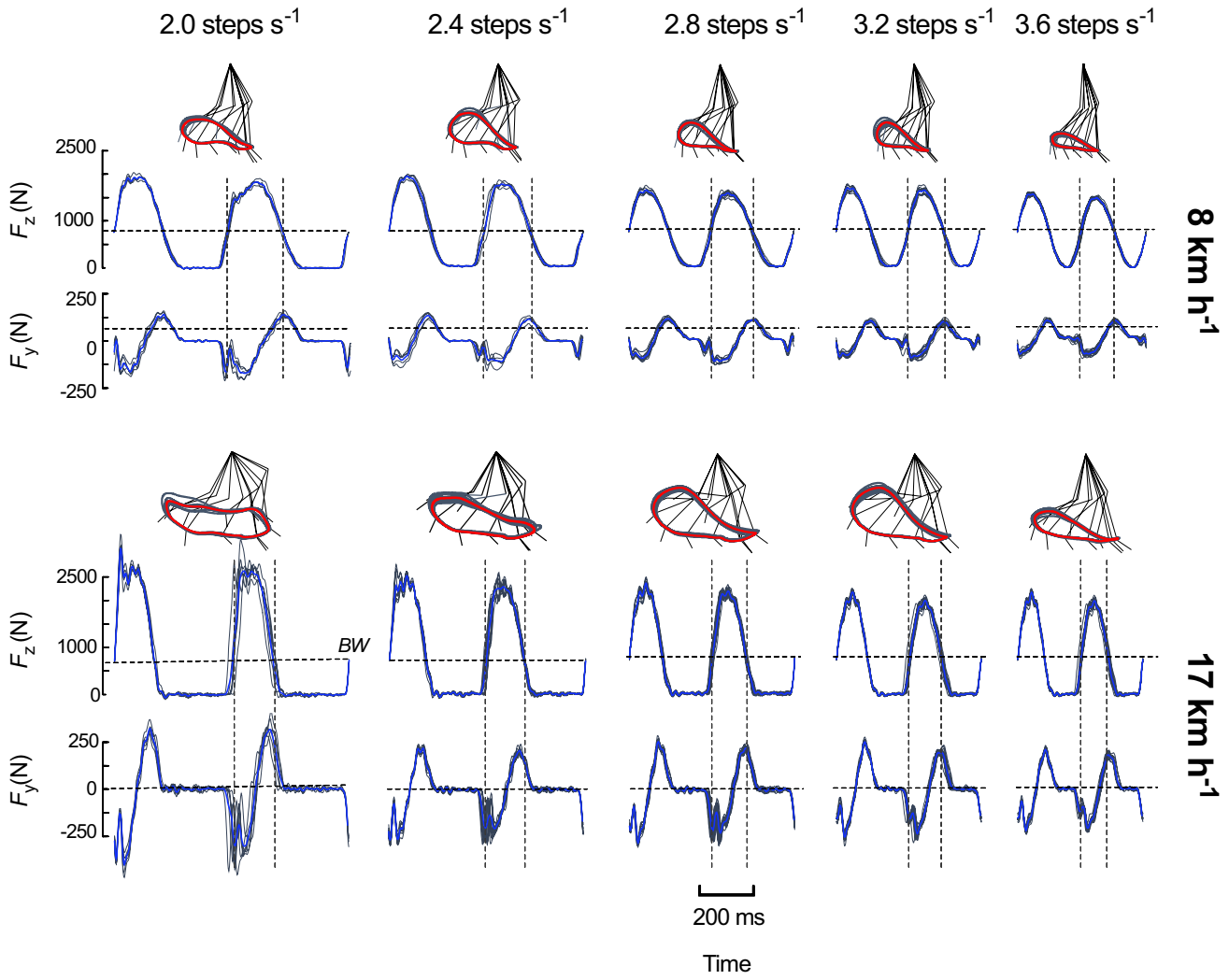

Fig. 1 (**A**) Average (blue) and individual (grey) time-curves of the fore-aft (F_f) and vertical (F_z) components of the GRF done by one subject at each step frequency (SF) class at 08 and 17 km h^{-1}. In the upper left corner of each panel, a stick diagram indicates the position of the limb-segments relative to the GT landmark every 10% of a stride. The loop illustrates the trajectory of the ankle relative to the GT over one stride

Figure 2A presents the time-curves of E_{kf}, E_v and E_{com} (blue curves) while running at 8 and 17 km h^{-1} in each frequency class. The positive external power done to move the CoM relative to the surroundings ($\dot{W}^{+}_{ext}$) is then calculated as the sum of the positive increments from the E_{ext}—curve over one stride (W^{+}_{ext}), divided by the time of the stride (Fig. 2B). The average power done during the push phase ($\dot{W}_{ext,push}$) is computed by dividing W^{+}_{ext} by the positive work phases, t_{push} (Table 2).

Computation of the internal power ($\dot{W}_{int}$)

The computation of the internal work done to accelerate and rotate the limbs relative to the CoM has been described in detail in Willems et al. (1995). Both legs were modelled as a multi-segmented limb formed by thigh, shank and foot segments. The upper body was modelled as a trunk, two arms and two forearm-hand segments (Dempster and Gaughran 1967). The internal energy of the *i*th segment is given by: $E^{i}_{int} = \frac{1}{2}\left(m_i V_i{}'^2 + I_i \omega_i^2\right)$ where m_i is the mass of the segment and I_i is its moment of inertia around its centre of mass, $V_i{}'$ is the translational velocity of the segment's centre of mass relative to the CoM and ω_i is the rotational velocity of the segment. The energy of the segments of the same limbs were added to obtain the energy of each limb. This procedure assumes that energy transfers are only possible between segments of the same limb, but not among the limbs (Dewolf et al. 2019; Willems et al. 1995). The internal energy time-curves (red curves) of the left and right upper-limbs (sum of upper-arm and lower-arm)

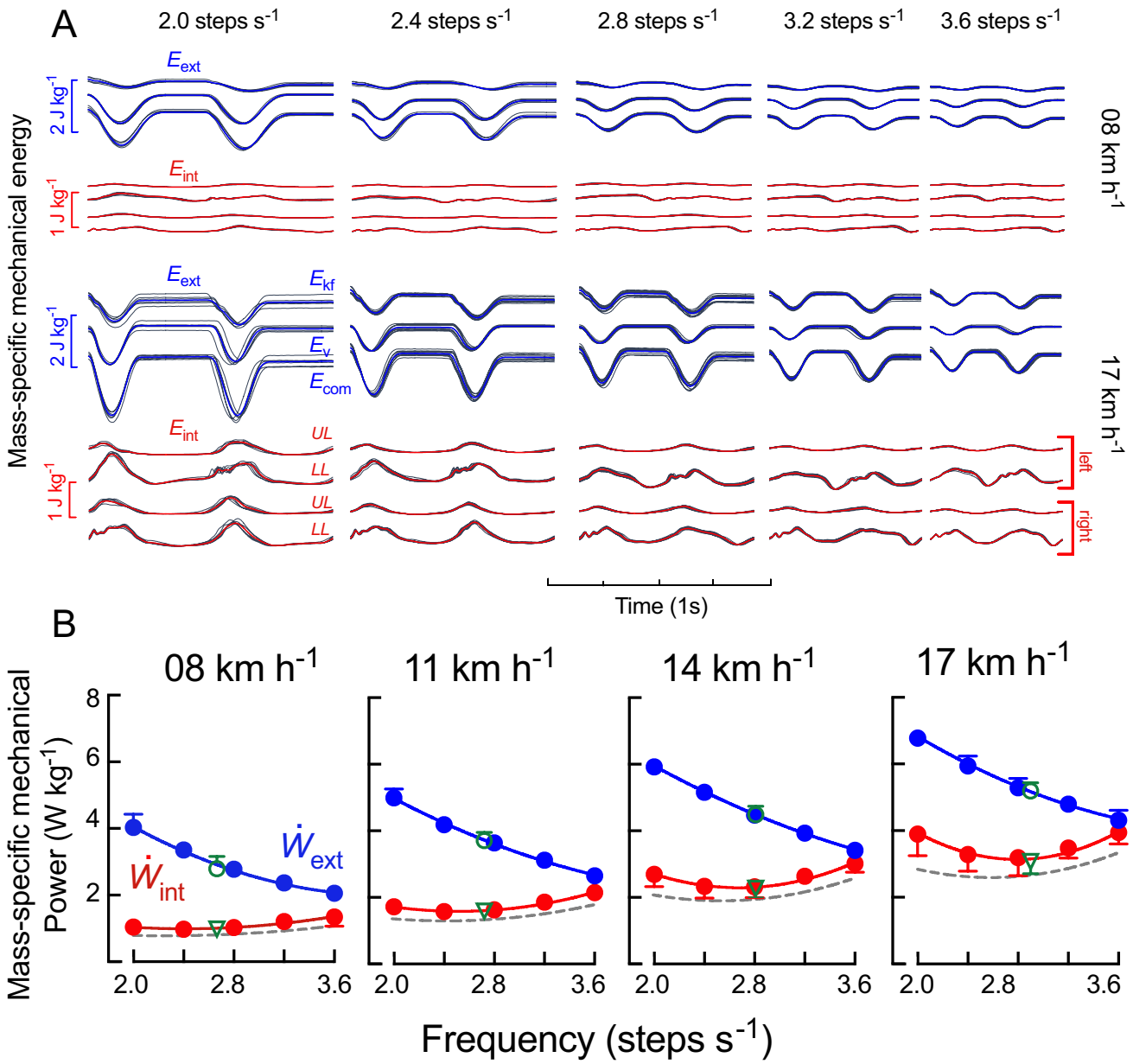

Fig. 2 (**A**) Average (blue) and individual (grey) time-curves of the normalised external energy done by the CoM (E_{com}), the energy done to sustain the movements in the vertical direction (E_v) and the energy done to sustain the movements in the fore- aft direction (E_{kf}) at each step frequency. The four red and corresponding grey time-curves represent respectively, from top to bottom, the normalised internal energy of the: left upper limb (UL), left lower limb (LL), right upper limb (UL) and right lower limb (LL) relative to the CoM for each SF at both 08 and 17 km h^{-1}. The grey contours in each panel correspond to the contact phases. Panel B shows the normalised mechanical external ($\dot{W}_{ext}$, blue circles) and internal ($\dot{W}_{int}$, red circles) power done by the CoM (W kg^{-1}) as a function of SF at different speeds. The points represent a grand mean and standard deviation at each step frequency. The green coloured open symbols represent the PSF grand mean and SD at different speeds. The grey dotted line represents the $\dot{W}_{int}$ of lower limb. The line which passes through all points is a quadratic non-linear regression as defined in Graphpad-Prism (Dotmatics, CA, USA)

and lower-limbs (sum of the thigh, shank and foot) while running at 8 and 17 km h^{-1} are presented in Fig. 2A. The positive internal power $\dot{W}^{+}_{int}$, Fig. 2B, is calculated as the sum of the positive increments of the internal energy of the four limbs divided by the stride time.

Computation of the mechanical stiffness

The mass-specific vertical stiffness (k_{vert}) was measured from the linear relation between a_v and S_v (Fig. 3). The slope of this linear relation was estimated as the ratio between the

Table 2 Average and standard deviation mass-specific push-averaged power (W kg^{-1})

Speed (km h^{-1})	2.0 (steps s^{-1})	2.4 (steps s^{-1})	PSF (steps s^{-1})	2.8 (steps s^{-1})	3.2 (steps s^{-1})	3.6 (steps s^{-1})
Mass specific push-averaged power $\dot{W}_{ext}$ (W kg^{-1}) (mean ± SD)						
8	12.51 ± 2.99	9.36 ± 1.44	7.08 ± 1.28	7.20 ± 1.15	6.17 ± 1.084	5.31 ± 1.27
11	17.76 ± 2.87	13.18 ± 1.56	11.02 ± 1.58	10.84 ± 0.77	8.79 ± 0.99	7.26 ± 1.26
14	23.61 ± 2.37	18.46 ± 1.97	14.62 ± 1.39	14.76 ± 0.70	12.11 ± 0.58	10.24 ± 1.12
17	29.25 ± 2.42	23.39 ± 2.35	18.11 ± 1.31	18.75 ± 1.23	16.10 ± 0.91	14.08 ± 1.18

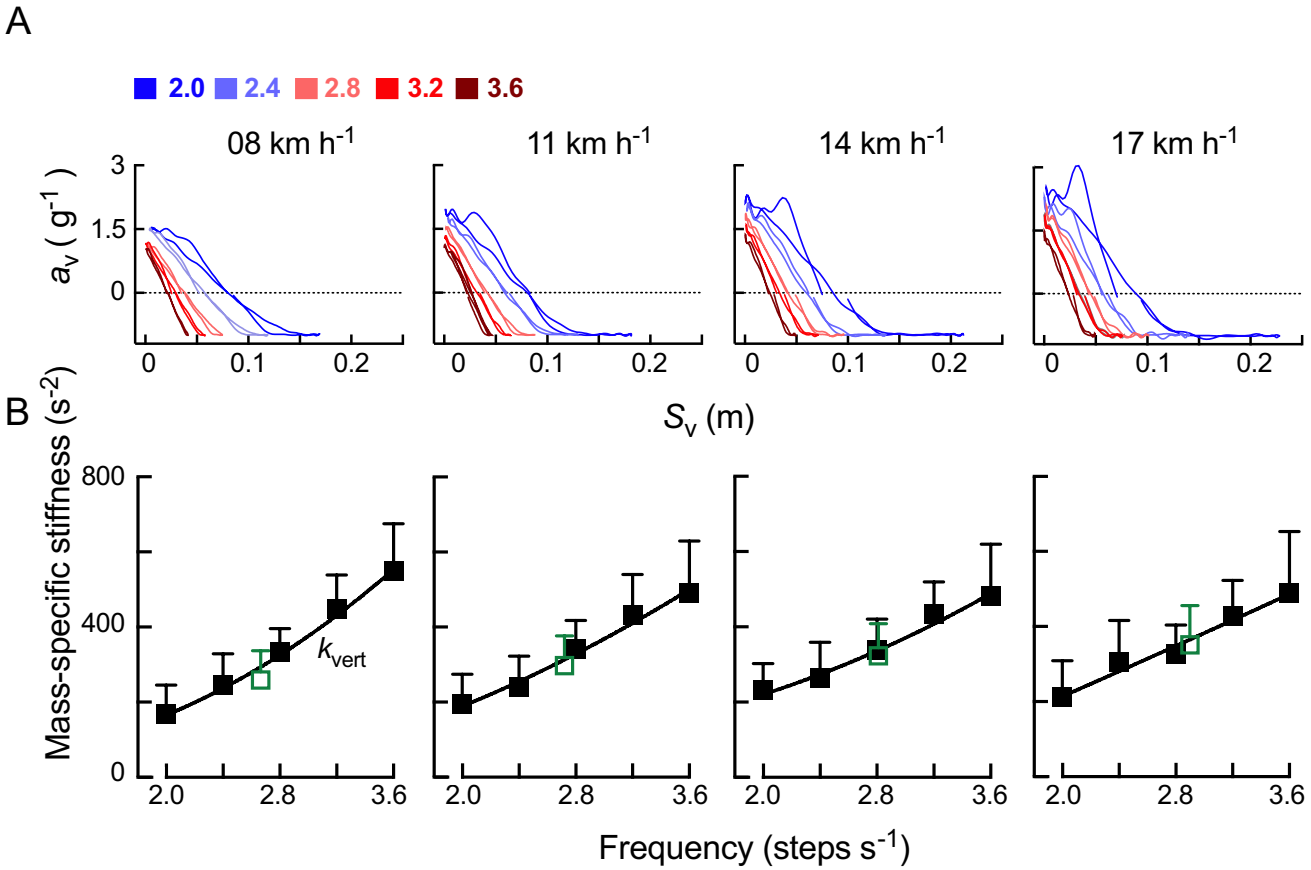

Fig. 3 (**A**) Acceleration of the CoM, a_v (g^{-1}), as a function of the vertical displacement (S_v) at different speed classes. Each curve represents a specific step frequency class. Note, the vertical stiffness (k_{vert}) of the CoM is characterised by the slope of each curve. Panel (**B**) shows k_{vert} as a function SF at different speed classes. All other indications are as in Fig. 2B

maximal vertical acceleration ($a_{v,max}$) of the CoM (whose event occurs close to the time at which the CoM reaches its lowest point) and the vertical displacement ($S_{v,ce}$) of the CoM during t_{ce} (Fig. 3): $k_{vert} = \frac{a_{v,max}}{S_{v,ce}}$.

Quantification of the intersegmental coordination via the planar covariance law

For each limb segment, the elevation angles ($\theta°$) in the sagittal plane (*i.e.,* the orientation of the segment in the sagittal plane relative to vertical) was computed by: $\theta = \arctan\left(\frac{z_p - z_d}{y_p - y_d}\right)$, where ($y_p$, z_p) and (y_d, z_d) are, respectively, the fore-aft (y) and vertical (z) coordinates of the proximal (subscript p) and distal (subscript d) markers of the segment. The joint angles (hip, knee, and ankle) were computed from the elevation angle of adjacent segments. The range of motion (ROM) during the stance and swing phases of each joint was computed as the difference

between the maxima and the minima of each joint waveform over each period.

The phase relationship between the three angles was assessed by computing the phase lag between each elevation angles and a cosine function (*xcorr* routine in Matlab). The difference in phase lag between the shank and foot segments elevation angles are presented in the results.

For each trial, time-curves of the elevation angles of the thigh, shank and foot were time-interpolated over individual strides to fit a normalised 800-point time-base. The elevation angles waveforms of the left leg were shifted by 50% of the stride period. A first average was done across left and right strides separately, then both legs were pooled together. In each condition, the average waveforms of the elevation angles of the three lower-limb segments: thigh, shank and foot were computed across participants.

In each speed-frequency class, the inter-segmental coordination of the lower-limb segments was assessed using principal component analysis (PCA). This procedure has been described in detail in the literature (e.g., Borghese et al. 1996; Catavitello et al. 2018; Daffertshofer et al. 2004; Dewolf et al. 2018) and will only be explained briefly here. The centred thigh, shank, and foot elevation angles waveforms once plotted in a three-dimensional space form a loop which lies close to a plane. The best fitting plane is the one generated by the first two components extracted by the PCA performed on the covariance matrix of the three elevation angles waveforms (Daffertshofer et al. 2004; Ivanenko et al. 2008). The PCA returns the matrix of eigenvectors U with its associated eigenvalues (λ_1, λ_2, λ_3) rank-ordered from the highest to the lowest. The eigenvectors u_1 and u_2 generate the best fitting plane and the third eigenvector, u_3, orthogonal to the first two, defines the orientation of the plane. The components of the u_3 vector: u_{3t}, u_{3s} and u_{3f} correspond to the direction cosines with the positive semi-axis of the thigh, shank and foot angular coordinates, respectively (Fig. 6). The percentage of variance associated to the u_3 vector ($PV_3 = \lambda_3 / (\lambda_1 + \lambda_2 + \lambda_3)$) was used as a planarity index ($PV_3 = 0\%$ for maximum planarity).

Statistics

For each participant, the dynamic parameters (*e.g.,* T, t_{ce} t_{ae}, L_{ce}, L_{ae}, k_{vert}) were averaged first across the right and left steps for each stride then averaged per stride, whereas the kinematic parameters (elevation angles, ROM, u_3, PV_3, etc.) were averaged directly across strides. Then descriptive statistical analysis was performed. First, the Shapiro–Wilk test was performed to verify normality. When the data did not meet the normal distribution criteria (Shapiro–Wilk's W-test, $p < 0.05$) non-parametric statistics were used for data analysis. A linear mixed effect model with *Bonferroni* post-hoc correction was used to assess the individual and interaction effects of frequency and speed on the calculated variables. When comparing means between two groups, for example when analysing the *on–off ground asymmetry,* a paired t test was used. Statistical tests were run on IBM SPSS Statistics (PASW Statistics, 19, SPSS, IBM, Armonk, NY, USA). The results of the statistical tests were considered significant for a p-value < 0.05. When a curve was drawn on figures, these were based on quadratic fits done on GraphPad Prism (GraphPad Software, LLC, Dotmatics, San Diego CA, USA).

Results

Effect of running frequency on the work and power done

External work and power

The external work done per step is much greater at low SFs than at high SFs ($p < 0.001$, fixed effect estimates between 2.0 and 3.6 steps s^{-1}: 0.71, $p < 0.001$; Fig. 2B). The mass-specific external power ($\dot{W}_{ext}$) is plotted in Fig. 2B, it decreases with speed and SF ($F_{fq} = 129.3$, $p < 0.001$). The push-averaged mechanical power ($\dot{W}_{ext,push}$) was also greater at fast running speeds ($p < 0.001$) and greater at smaller SF as compared to higher SF ($F_{fq} = 16.7$, $p < 0.001$) (Table 2).

Internal work and power

The internal positive power increases when deviating from PSF (Fig. 2). Indeed, for each speed, the positive internal power is at its minimum between ± 2.4 and ± 2.8 steps s^{-1} (the *minima* are 2.39, 2.52, 2.68, 2.79 steps s^{-1}, respectively, at 8, 11, 14 and 17 km h^{-1}, based on a polynomial regression curve in Fig. 2B). The increase in W_{int} is greater when running at higher SFs and low SFs compared to PSF ($F_{fq} = 728.2$, $p < 0.001$). Furthermore, the internal power ($\dot{W}_{int}$), as seen in Fig. 2, increases with both speed and frequency ($F_{fq} = 24.2$, $p < 0.001$). However, when analysed separately, we observed that the upper limb $\dot{W}_{int}$ increases with speed but decreases with frequency ($F_{fq} = 18.45$, $p < 0.001$).

Bouncing mechanism of running

Vertical stiffness

Figure 3 illustrates the vertical GRF plotted as a function of the vertical displacement of the COM, showing a quasi-linear relationship. The mass-specific vertical stiffness was reduced with lower SF and increased with higher SF ($p < 0.001$, Fig. 3). At the PSF, k_{vert} increases with speed as in Cavagna et al. (1988), whereas throughout the

frequency classes, k_{vert} does not vary much with speed. The increase of vertical stiffness is related to the vertical force applied to the ground. Indeed, the $F_{v,max}$ is greater at low SF as compared to high SF ($F_{fq} = 956.9$, $p < 0.001$; Fig. 1).

On–off ground asymmetry

When running at an imposed step frequency, the speed can only be changed by tuning the step length, L (Fig. 4). At a frequency of 2 step s^{-1}, L varies from ~ 1.1 m at 8 km h^{-1} to ~ 2.4 m at 17 km h^{-1}. The horizontal distance covered by the CoM during t_{ce}, *i.e.* L_{ce} ranges from 0.5 m at the lowest

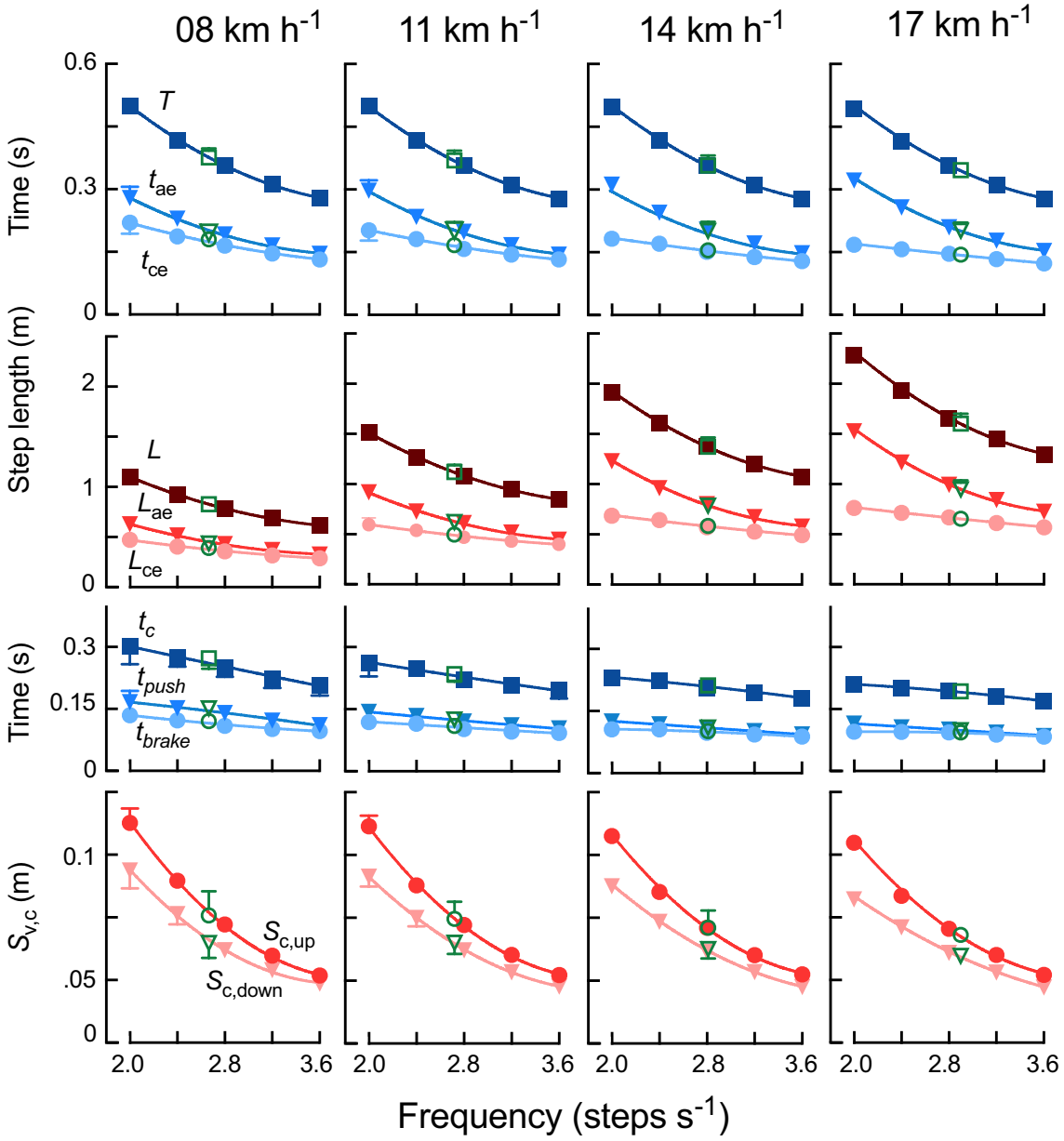

Fig. 4 Spatiotemporal and step length parameters presented as a function of SF at different speed classes. The upper row presents the step time (T, dark blue squares), effective aerial time (t_{ae}, light blue circles) and effective contact time (t_{ce}, light blue triangles). The second row represents the corresponding step length (L, dark red squares), effective aerial length (L_{ae}, light red triangles) and effective contact length (L_{ce}, pink circles). The third and fourth rows show the spatiotemporal parameters and vertical displacement of the CoM, both occurring during the contact phase (t_c). In the top row, the t_c (dark blue squares) is divided into its brake (t_{brake}, light blue circles) and push phases (t_{push}, light blue triangles). In the bottom row the vertical displacement of the CoM during the contact phase is divided into the displacement done between the touch down and minimum height ($S_{c,down}$, pink triangles) and from the minimum until take-off height ($S_{c,up}$, red circles). All other indications are as in Fig. 2B

speed to 0.75 m at the highest speed, close to the maximal anatomical value previously determined by Cavagna et al. ~ 0.7 m (1991). Since L_{ce} is limited, L is increased by increasing L_{ae} (L–L_{ce}). When speed increases, the period t_{ce} to cover the distance L_{ce} decreases and consequently, t_{ae} (T–t_{ce}) must increase accordingly. Subsequently, when running at low SFs, the bounce is asymmetric at all speeds, *i.e.,* $L_{ce} < L_{ae}$ and $t_{ce} < t_{ae}$ (for t_{ce}, $t_{ae:}$ $p < 0.007$ and for L_{ce}, L_{ae}: $p < 0.002$ at slow speeds) and this asymmetry is more pronounced the higher the speed (for t_{ce}, t_{ae} and for L_{ce}, L_{ae}: $p < 0.001$ at fast speeds).

At 3.6 step s^{-1}, L varies from ~ 0.6 m at 8 km h^{-1} to ~ 1.3 m at 17 km h^{-1}. At this frequency, L_{ce} ranges from 0.3 m at the lowest speed and 0.6 m at the highest speed, which is smaller than the anatomical limitation. For most speeds, $L_{ce} = L_{ae}$ ($p > 0.05$), and in turn $t_{ae} = t_{ce}$ ($p > 0.05$), except at 17 km h^{-1} where it becomes slightly asymmetric ($p < 0.001$ for both). Therefore, when running at a higher frequency, the bounce is symmetric in a larger range of speeds.

Landing-take off asymmetry

The timing of negative and positive work production during t_c varies with speed and step frequency (Fig. 4). In particular, t_{push} is modified by the SF ($F = 776.4$, $p < 0.001$). Indeed, the timing during which muscles perform positive external work is extended during running with a lower SF while it is decreased at a higher SF ($F = 776.4$, $p < 0.001$). This landing-take off asymmetry is also reflected in the displacement of the COM during the contact phase. At low SFs and slow running speeds, the vertical downward displacement of the COM, $S_{c,down}$, is greater than its upward counterpart (Fig. 4), this difference lessens with increasing speed and SF.

Kinematics of running

Intersegmental coordination. Figure 5 illustrates the time-normalised elevation angular motion waveforms of the thigh, shank and foot over an entire stride at 8 and 17 km h^{-1} and in all frequency classes. Below each group of curves is depicted the corresponding, 3-dimensional view of the elevation angle trajectories along with the best fitting plane. At each speed, an increase of the step frequency corresponds to a rotation of the covariation plane (*i.e.,* when reading Fig. 5 from left to right), whereas maintaining a fixed step frequency and increasing the speed (*i.e.,* reading from top to bottom), the rotation is no longer evident. This is further shown in Fig. 6, where u_{3t}, the direction cosine of the third eigenvector which is orthogonal to the plane, increases with frequency but not with speed ($F_{fq} = 22.9$, $p < 0.001$; speed: $p = 0.8$). It can also be observed that at 2 step s^{-1}, the shape of the loop is drastically different from the other conditions and is speed dependent, changing from a drop-like shape at 8 km h^{-1} to a quasi-ellipse at 17 km h^{-1}, while at the other conditions the only observation is an enlargement of the loop whilst keeping a similar shape. u_{3s} slightly decreases with SF ($F = 5.44$, $p < 0.001$) and does not change with speed ($p = 1$). Concerning u_{3f}, there is a slight effect of SF ($F = 2.9$, $p = 0.02$) and of speed ($p < 0.001$). The latter is because there is a difference between 8 km h^{-1} and the other speeds (fixed effect estimate − 0.32, $p < 0.014$, compared to 17 km h^{-1}).

The percentage of variance accounted for by the third eigenvector (PV_3) was used to quantify the planarity. Results show that the planarity was generally maintained for all speed and frequency classes (PV_3 ranged between 1.3% and 3.6%, overall minimum and maximum values, respectively). Linear mixed model effect shows a slight interaction effect between the speed of progression and frequency ($p = 0.007$). However, when considering post-hoc correction PV3 is significantly lower at speeds above 14 km h^{-1} ($p < 0.001$) as compared to slower speeds. Furthermore, PV3 is lower at SFs below 2.8 steps s^{-1} compared to PSF ($p < 0.001$).

At 2.0 step s^{-1}, the movements of the shank and the foot are not in phase. When speeds and frequencies increase, the phase shift between the shank and foot elevation angles tends towards 0 meaning the movements of these two segments become gradually in phase (SF: $F = 10.6$, $p < 0.001$; speed: $p = 0.127$). The phase relationship between the thigh and shank elevation angles decreases with speed ($p < 0.001$) and increases at the lowest frequencies as compared to PSF (SF: $F = 7.58$, $p < 0.001$).

Both the amplitude ratio and the time relationship characteristics between the elevation angles of two adjacent limb segments determine the lower-limb joint angle. For example, if the shank and foot elevation angles have the same amplitude and are in phase, no motion would occur at the level of the ankle. Therefore, since a joint angle can be deduced from two adjacent elevation angles, the joint angles and their ROM are only presented in supplementary materials (Figs. S1 and S2).

Discussion

The effect of step frequency on the bouncing mechanism

When running speed increases, the PSF increases from 2.7 steps s^{-1} at 2.2 m s^{-1} to 2.9 steps s^{-1} at 4.7 m s^{-1}. Already well-documented in the literature (He et al. 1991; Cavagna et al. 1988), we observed an effect of speed on the vertical stiffness at PSF. Regarding a change in frequency at a given speed, a linear relationship between k_{vert} and SF has been documented at only one relatively slow speed of progression (i.e., 2.5 m s^{-1}) by Farley and González (1996). Here, by analysing various speed classes, we highlight

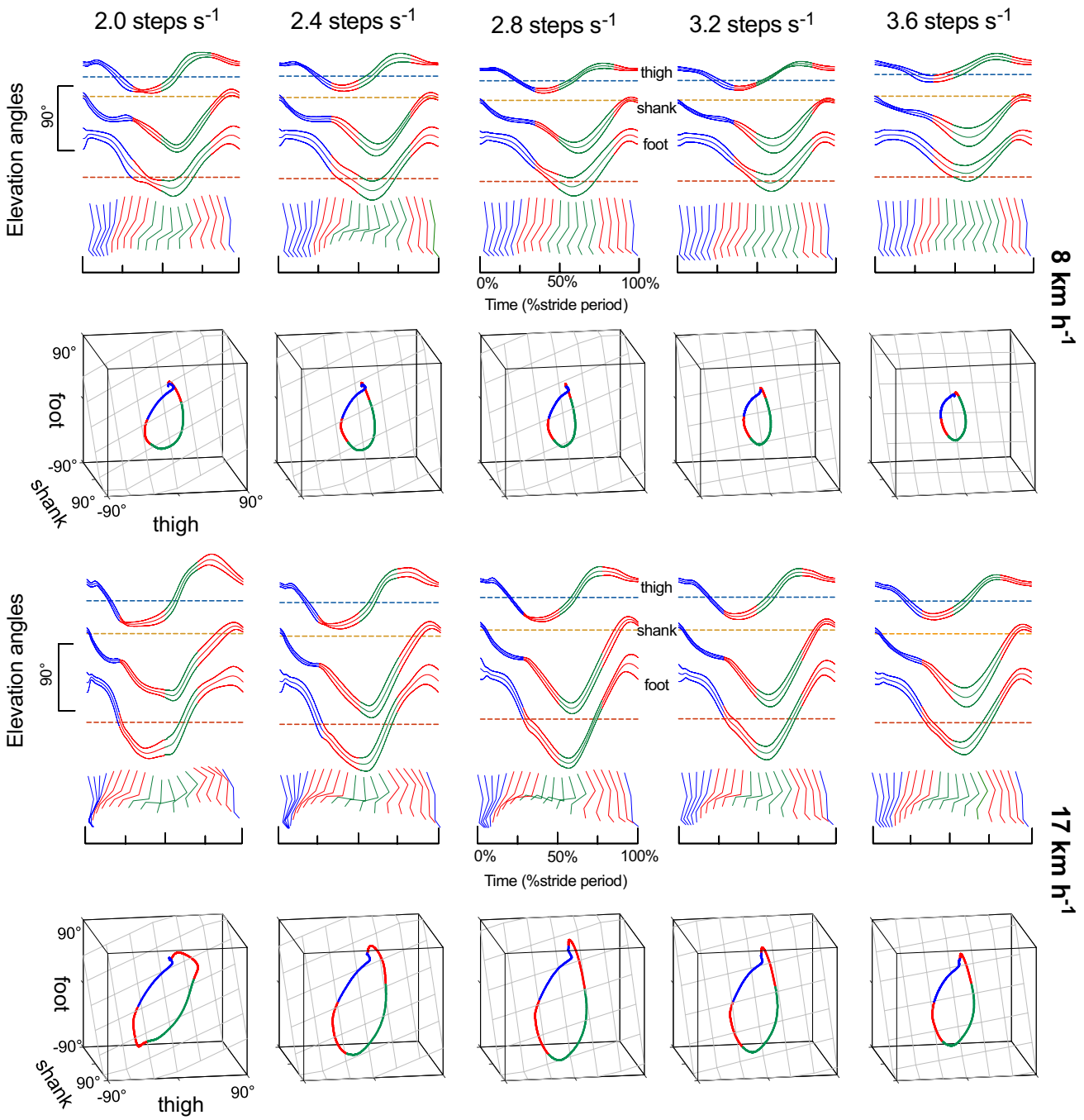

Fig. 5 Time normalised average ± standard deviation cloud of the lower limb elevation angles done over a percentage of stride at different SF presented at both 08 and 17 km h^{-1}: thigh (top), shank (middle), and foot (bottom). The stride is cut into their four sequential temporal parts. (1) Blue corresponds to the contact time, followed by (2 and 4) the aerial phases in red, (3) the green represents the contact time of the other leg. The horizontal, respectively, coloured, dashed line represents the neutral standing position of each segment. The stick figures below represent a typical trace of one subject taken every 5% of the stride, the colours represent the same temporal phases as the elevation angles. The cubes below show the average loop trajectories across all participants with superimposed the best fitting covariance planes (the grey grids)

another important finding. In each speed class, k_{vert} increases similarly with SF as observed in Farley & González. This result suggests that the adaption of k_{vert} to a particular speed reflects a change in the frequency chosen by the runner more than a change in the running speed itself. This is evidenced by the 'sliding' of the PSF values upon the frequency curves at different speed classes for k_{vert} as shown by the green square dots in Fig. 3B.

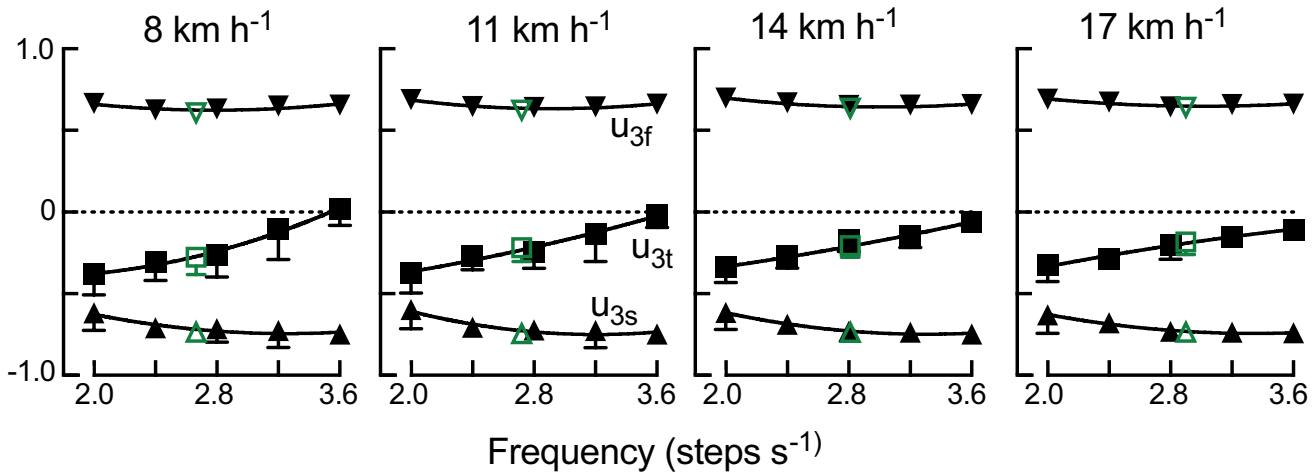

Fig. 6 The third eigenvector direction cosines for the thigh (u_{3t}, squares), shank (u_{3s}, upper triangles) and foot (u_{3f}, downwards triangles) segments, of the normal to the covariation plane as a function of SF at different speeds. All other indications are as in Fig. 2B

Similarly, the observation is also valid for the orientation of the covariance plane, which reflects the coordination between the lower-limb segments. Indeed, at the PSF an effect of speed has been observed or so, the orientation of the plane rotates as a function of speed (Ivanenko et al. 2007). However, as for k_{vert} when considering the whole data set of speeds and frequencies, we observed an increase of u_{3t} as a function of SF but not as a function of running speed. In other words, the effect of speed on u_{3t} at PSF could simply be due to a change in the preferred step frequency across speeds.

The choice of PSF, at the speeds studied in this paper, has been shown to be self-optimised by runners in a way that minimises both the mechanical and metabolic power of the runner (Burns et al. 2019; Cavagna et al. 1991). This is a central element in the development of an economical and safe running gait (Folland et al. 2017; Moore 2016; Williams and Cavanagh 1987). As explained in the recent review by Van Oeveren et al. (2021), debate exists whether SF is modified within trained/elite runners as compared to recreational/amateur runners: some authors show an increase of SF in athletes (Nuñez Lisboa 2021; Slawinski and Billat 2004), others find a decrease (da Rosa et al. 2019) and still others find no significant differences between groups (Folland et al. 2017). In fact, the choice of PSF is highly dependent on the speed of progression, however, better runners are shown to have a resonant step frequency (*i.e.,* the natural frequency of the bouncing system) (Cavagna et al. 1991) that is increased as compared to amateur runners, as argued in da Rosa et al. (2019).

Running with a high step frequency

As described in Cavagna (2010), running with a step frequency higher than the PSF requires lower GRFs per step, both in the fore-aft and vertical direction (Fig. 1). Thus, the external work and power (Fig. 2) done to move the CoM is also decreased. On the contrary, the internal power,$\dot{W}_{int}$, to move the limbs relative to the CoM is increased as the time required to reset the limbs for the following step is shorter and the limbs must be reset more often for the same time period.

From a mechanical point of view, running with a higher step frequency seems to accentuate the elastic bounce of running. Indeed, the spring becomes stiffer as the vertical displacement is smaller and both the contact (t_c) and effective (t_{ce}) contact times are smaller (Farley and González 1996). Furthermore, producing smaller steps is also done by reducing the effective aerial phase (t_{ae}), which becomes shorter (Fig. 4). We observe here that the subjects spontaneously adopt a *symmetric rebound*, where the duration of the lower part and upper part of the vertical oscillation is about equal and the step frequency equals the natural frequency of the bouncing system (Cavagna et al. 1988). According to Cavagna (1997), tuning the step frequency to the natural frequency of the bouncing system results in a minimum of metabolic energy expenditure and in a maximum of the efficiency of conversion of stored energy into positive work.

The accentuation of the 'elastic bounce' in human running shows smaller differences between the 'braking phase', where elastic energy is stored into the muscle–tendon unit, and during the 'push phase', where elastic energy is released

(Cavagna 2009; Dewolf and Willems 2017, 2019; Ruina et al. 2005). First, the difference observed between the downward and upward displacements of the CoM during contact is reduced at higher SFs (Fig. 4), suggesting a smaller hysteresis in the force–length relationship of the spring leg. Second, the duration of the positive work production phase, t_{push} becomes similar to that of the negative work production phase, t_{brake}. The bounce of an elastic structure with no hysteresis would imply a $t_{push} \approx t_{brake}$ and $S_{c,down} \approx S_{c,up}$ (Cavagna 2009); therefore the modifications observed at high SFs are an expression of a more efficient use of elastic rebound, *i.e.,* that the positive energy released approaches the negative energy stored. Nevertheless, when SF increases, the more efficient elastic rebound translates to less external work produced by the transformation of chemical energy into mechanical work but also comes with an increase of the internal work (Cavagna et al. 1991).

From a kinematic point of view, to perform a smaller step length, the ROM of the lower limb segments (elevation angles) and consequently of the joints is adapted. The reduction of step length with higher SF induces a reduction of the thigh elevation angle ROM (and in turn of the hip ROM) during both the contact and aerial phases (Fig. 5 and Fig. S1). Furthermore, the ROM of the knee reflects the modifications brought about the amplitude and timing relationship of the thigh and shank segment elevation angles (Fig. S1 and Fig. 5). During the contact phase, the knee ROM decreases to control the vertical stiffness of the lower limb (Ferris and Farley 1997; Günther and Blickhan 2002). During the aerial phase, it has been reported that runners with a higher SF have higher knee flexion during the swing phase (van Oeveren et al. 2021). At first glance, our results (Fig. S2) would disagree with these findings, however, at the speeds measured in this study, the normal ranges of PSF are on average always below 3 steps s^{-1} (Table 1). When the SF rises above 3 steps s^{-1} the time required for the aerial phase is too short for a runner to fully swing their leg and adequately bend their knee. Consequently, knee ROM decreases at higher SFs, despite its negative consequences on the W_{int} (Fig. 2). Additionally, as step length increases, the phase relationship between shank and foot segments elevation angles tend to 0 (Fig. 5) and ankle motion decreases. It has been noted that ankle motion is primarily a consequence rather than a cause of leg motion (van Oeveren et al. 2021). Moreover, this reduction in ROM during the contact phase, as frequency increases, may contribute to the reduction of the *landing-take-off* asymmetry (Maykranz and Seyfarth 2014).

In addition to the modifications of joint angles, the changes in the phase relationships between the elevation angles of the lower limb segments are evidenced by changes in the third eigenvector, and in particular u_{3t} (Barliya et al. 2009; Bianchi et al. 1998). The eigenvector direction cosine, u_{3t} tends towards zero at the highest SF which is most likely due to the reduction of the distance between the minima of the foot and shank segments that are more in-phase (Figs. 5 and 6). Because of the reduction of movement amplitude, we also observe that the loop amplitude decreases with increasing step frequency (Fig. 5).

Running at a low step frequency

Running with a step frequency lower than the PSF requires greater GRF in both the fore-aft and vertical direction to travel (Fig. 1), thus increasing the external work (and, therefore, the external power, Fig. 2). In turn, the internal power done over the step, $\dot{W}_{int}$, is reduced as the time to reset the limb is longer and the limbs must be reset less often per unit time (Fig. 2). However, at the lowest SFs $\dot{W}_{int}$ increases after reaching a minimum.

From a mechanical point of view, running with a step frequency lower than the PSF seems to lessen the effectiveness of the elastic rebound at any speed. Indeed, k_{vert} is reduced as the vertical displacement and the effective contact time (t_{ce}) increase. Furthermore, at a given speed for a runner to increase *SL*, they must lengthen both L_{ae} and L_{ce} until the latter reaches its physiological limit (~0.6–0.7 m) (Cavagna et al. 1988, 1991, 1997) (Fig. 4). Beyond this point, the only way of increasing *L* is by increasing L_{ae}. As a result, $t_{ce} < t_{ae}$ and the subjects adopt an *asymmetric rebound*.

The t_{ae}, t_{ce} asymmetry implies that the velocity at take-off and so the power produced during t_{push} must be increased. A greater push-averaged power ($\dot{W}_{ext,push} = W_{ext}/t_{push}$) is therefore observed (Table 2). This is similar to uphill running or running against a horizontal traction force, where the push-average power must be increased (Dewolf et al. 2016; Mesquita et al. 2020), the increase of power is limited by (i) increasing the duration of the push at the expense of the duration of the brake (Fig. 4), and (ii) by reducing the downward displacement of the CoM as compared to its upward motion.

Running at a low SFs has consequences on the kinematic strategies adopted by the subject as evidenced partly by the larger and quasi-ellipse shaped loop (Fig. 5). Due to changes in the phase relationships between the elevation angle waveforms of the lower limb segments, the changes in u_{3t}, (Figs. 5 and 6) are evidence of an adapted kinematic strategy (plane rotation) when reducing SF. Particularly, u_{3t} decreases with lower SF, while u_{3s} decreases and u_{3f} remains relatively constant. Moreover, u_{3t} has been correlated with the mechanical energy expenditure during walking (*i.e.,* the higher the third eigenvector, the higher the net mechanical power) (Borghese et al. 1996; Grasso et al. 2000). This could imply that the rotation of the covariance plane is correlated with the net mechanical power produced to move the CoM in running. At slower step frequencies, the third eigenvector

is furthest from 0, *i.e.,* the plane rotates considerably at such SFs, potentially related to the fact that the net mechanical power developed to move the CoM forward is increased (Figs. 2, 5 and 6).

The lower limb and joint motion at touchdown have been reported to be similar at the level of the thigh, the knee and ankle for SFs ranging from 2.5 to 3.1 steps s^{-1} (Clarke et al. 1985). Whereas we also observed little to no modification at touchdown, the ROM during the contact phase is influenced by the SF. For example, the longer steps are a consequence of a modification of the thigh oscillation (and in turn the hip) during the contact phase (Fig. 5 and S2), even if this increase is limited by anatomical factors. A consequence of such limitations is that the thigh ROM increases mainly during the aerial phase. In addition, during the contact phase, the knee ROM increases as the vertical displacement increases, indirectly controlling the reduction of lower limb stiffness with low SF. Concerning the ankle joint, the ROM during the contact phase also increases as SF decreases. The greater joint ROM, reflects the modification of the phase relationship between shank and foot segment elevation angles, may reflect a greater contribution of the muscle to the length change of the muscle–tendon unit during contact, thus deviating from an elastic rebound (Fig. 5, S2).

During the swing phase, the subject sees their aerial peak knee flexion (and in turn the $ROM_{ta,}$ Fig. S2) decrease as the SF decreases. A smaller knee flexion throughout the aerial phase leads to an increased inertia of the swing leg over the aerial phase (Willems et al. 1995). A greater swing leg moment could be used by the runner as a supplementary upwards impulse to the stance leg as it pushes off the ground (Seyfarth et al. 2022), to increase the propulsive forces in the fore-aft direction that are associated with running at lower SFs (Cavagna et al. 1991; Chang and Kram 1999).

Observations regarding the W_{int}

When considering for energy transfer between the segments of the same limb, our W_{int} results at PSF are, respectively, on average 12% and 14% lower than the results obtained in Willems et al. (1995) and Cavagna et al., (1991) which were done while over-ground running but similar to Gosseye et al. (2010) done while running on a treadmill. However, when not taking energy transfer between segments into account, our results are on average only 2.5% lower to those of Willems and colleagues. This difference could be due to differences in movements of the limbs on a treadmill as compared to over-ground running (Miller et al. 2019; Van Hooren et al. 2020). In contrast with the results of Cavagna et al. (1991), our results show that the $\dot{W}^{+}_{int}$ does not decrease linearly with decreasing SF. Here we observe that the internal work reaches a minimum at around 2.4 steps s^{-1} before rising again, especially at fast running speeds. These authors base this result on lower speeds. In fact, at the faster speeds the internal work was only measured at higher SFs (smallest SF 2.5 steps s^{-1} at 14 km h^{-1} and 3.2 steps s^{-1} at 17 km h^{-1}) and a regression curve was used to extrapolate the lower internal work results. Here, at low SF a greater contribution of the upper limbs increases the $\dot{W}^{+}_{int}$ compared to PSF (Fig. 2A, B). This is visible in Fig. 2B as the difference between the power done by the lower limbs (dashed grey line) and the total $\dot{W}^{+}_{int}$ (red lines and circles). In addition, due to the greater knee extension during stance (Fig. S1), the maximal velocity of the foot is greater at low SF as more distance needs to be travelled during the swing phase (Fig. S3). Both the ipsilateral arm and the contralateral swing leg could be used by the runner as a supplementary upwards impulse to the stance leg (Seyfarth et al. 2022).

During a stride, the internal energy-time curve of each lower limb, as seen in Fig. 2, presents two peaks occurring during the two contact phases: a first peak when the lower limb itself is in contact with the ground and moves backwards relative to the trunk, a second peak when the opposite lower limb is in contact with the ground. In this case, the lower limb moves forwards relative to the trunk. During the two aerial phases, the internal energy of each limb is minimal, suggesting that the limbs are not moving a lot relative to the CoM. A similar phenomenon is observed at the level of the upper limbs: the kinetic energy of the upper limbs relative to the COM is higher during the contact phases than during the aerial phases. Although, due to the small mass of the upper limbs, the variation of their internal energy is smaller than in the lower limbs.

A proper synchronisation between the movements of the upper and lower limbs during running can be beneficial in terms of energetics and gait stability in locomotion. In the discussion of Willems et al. (1995), the authors argue that it is rather complicated to consider for energy transfer between the energy of the limb segments and the energy of the CoM without regarding for the feasibility of this transfer. The peaks present in the energy curves of the limb segment movements which correspond to the energy curve peaks based on the movements of the CoM could be evidence that a transfer between limb segment energy and CoM energy is in fact possible.

Limitations

Some limitations are present in this paper. First, although the required number of steps is met to be able to reduce type I error, the sample size is rather small. Furthermore, all subjects were recreational amateur runners. The study did not compare untrained and trained runners whereas a lot of the literature distinguishes two groups. Second, the difference in our findings and the findings from Cavagna

et al (1991) concerning the W_{int} at the lowest frequencies and faster speeds do not match. This difference could be due to a result of the instruments used in data acquisition and analysis. Another possibility is that there are differences between the internal work of a subject when running overground and on a treadmill *e.g.,* eventual energy transfers between internal and external work. This last limitation should, therefore, not be viewed as a limitation per se but rather as a starting point for further research comparing the differences between both.

Conclusion

To the best of our knowledge, this paper is the first, to compare SF and the bounce mechanics' spatiotemporal parameters and its relation to lower limb motion. Despite the extensive literature on SF and running, our results bring arguments that the adaption of k_{vert} to a particular speed reflects a in the frequency chosen by the runner more than the running speed itself. This result is also extended to the motion and relation of the lower limb segments, as evidenced by the planar covariance law. When running at higher SF, running mechanics is best explained by the elastic bouncing model of running. Whereas when running at the lower SFs, running mechanics thus deviates from the bouncing model of running.

Supplementary Information The online version contains supplementary material available at https://doi.org/10.1007/s00421-023-05303-3.

Acknowledgements The authors would like to thank F. Desimpelaere for her contribution in the data collection and treatment during her time at the lab.

Author Contribution PW and RM conceived and designed research. RM and GC conducted experiments. GC, RM and AD analyzed data. RM, PW, GC, and AD contributed to the interpretation of the results. RM and AD wrote the first draft of the manuscript. All authors provided critical feedback and helped shape the research, analysis and manuscript.

Funding Fonds De La Recherche Scientifique - FNRS. Grant number CDR 40013847. Pr. Arthur Dewolf.

Data availability Data are available upon reasonable request.

Declarations

Conflict of interest The authors declare no conflict of interest.

References

Barliya A, Omlor L, Giese MA, Flash T (2009) An analytical formulation of the law of intersegmental coordination during human locomotion. Exp Brain Res 193(3):371–385. https://doi.org/10.1007/s00221-008-1633-0

Bianchi L, Angelini D, Orani GP, Lacquaniti F (1998) Kinematic coordination in human gait: relation to mechanical energy cost. J Neurophysiol 79(4):2155–2170. https://doi.org/10.1152/jn.1998.79.4.2155

Blickhan R (1989) The spring-mass model for running and hopping. J Biomech 22(11–12):1817–1227

Borghese NA, Bianchi L, Lacquaniti F (1996) Kinematic determinants of human locomotion. J Physiol 494(3):863–879. https://doi.org/10.1113/jphysiol.1996.sp021539

Burns GT, Zendler JM, Zernicke RF (2019) Step frequency patterns of elite ultramarathon runners during a 100-km road race. J Appl Physiol 126:462–468

Catavitello G, Ivanenko YP, Lacquaniti F (2015) Planar covariation of hindlimb and forelimb elevation angles during terrestrial and aquatic locomotion of dogs. PLoS ONE 10(7):e0133936. https://doi.org/10.1371/journal.pone.0133936

Catavitello G, Ivanenko Y, Lacquaniti F (2018) A kinematic synergy for terrestrial locomotion shared by mammals and birds. Elife 7:e38190. https://doi.org/10.7554/eLife.38190

Cavagna GA (2009) The two asymmetries of the bouncing step. Eur J Appl Physiol 107(6):739–742. https://doi.org/10.1007/s00421-009-1179-2

Cavagna GA (2010) Symmetry and asymmetry in bouncing gaits. Symmetry 2(3):1270–1321. https://doi.org/10.3390/sym2031270

Cavagna GA, Franzetti P, Heglund NC, Willems P (1988) The determinants of the step frequency in running, trotting and hopping in man and other vertebrates. J Physiol 399(1):81–92. https://doi.org/10.1113/jphysiol.1988.sp017069

Cavagna GA, Willems PA, Franzetti P, Detrembleur C (1991) The two power limits conditioning step frequency in human running. J Physiol 437(1):95–108. https://doi.org/10.1113/jphysiol.1991.sp018586

Cavagna GA, Mantovani M, Willems PA, Musch G (1997) The resonant step frequency in human running. Pflugers Arch 434(6):678–684. https://doi.org/10.1007/s004240050451

Chang Y-H, Kram R (1999) Metabolic cost of generating horizontal forces during human running. J Appl Physiol 86(5):1657–1662. https://doi.org/10.1152/jappl.1999.86.5.1657

Clarke TE, Cooper LB, Hamill CL, Clark DE (1985) The effect of varied stride rate upon shank deceleration in running. J Sports Sci 3(1):41–49. https://doi.org/10.1080/02640418508729731

Courtine G, Roy RR, Hodgson J, McKay H, Raven J, Zhong H, Yang H, Tuszynski MH, Edgerton VR (2005) Kinematic and EMG determinants in quadrupedal locomotion of a non-human primate (Rhesus). J Neurophysiol. https://doi.org/10.1152/jn.01073.2004

da Rosa RG, Oliveira HB, Gomeñuka NA, Masiero MPB, da Silva ES, Zanardi APJ, de Carvalho AR, Schons P, Peyré-Tartaruga LA (2019) Landing-takeoff asymmetries applied to running mechanics: a new perspective for performance. Front Physiol 10:415. https://doi.org/10.3389/fphys.2019.00415

Daffertshofer A, Lamoth CJC, Meijer OG, Beek PJ (2004) PCA in studying coordination and variability: a tutorial. Clin Biomech 19(4):415–428. https://doi.org/10.1016/j.clinbiomech.2004.01.005

Dempster WT, Gaughran GRL (1967) Properties of body segments based on size and weight. Am J Anat 120(1):33–54. https://doi.org/10.1002/aja.1001200104

Dewolf AH, Willems PA (2017) A collision-based analysis of the landing-takeoff asymmetry during running. Comput Methods Biomech Biomed Engin 20(sup1):65–66. https://doi.org/10.1080/10255842.2017.1382863

Dewolf AH, Willems PA (2019) Running on a slope: A collision-based analysis to assess the optimal slope. J Biomech 83:298–304. https://doi.org/10.1016/j.jbiomech.2018.12.024

Dewolf AH, Peñailillo LE, Willems PA (2016) The rebound of the body during uphill and downhill running at different speeds. J Exp Biol 219:2276–2288. https://doi.org/10.1242/jeb.142976

Dewolf AH, Ivanenko Y, Zelik KE, Lacquaniti F, Willems PA (2018) Kinematic patterns while walking on a slope at different speeds. J Appl Physiol 125(2):642–653. https://doi.org/10.1152/japplphysiol.01020.2017

Dewolf AH, Ivanenko YP, Zelik KE, Lacquaniti F, Willems PA (2019) Differential activation of lumbar and sacral motor pools during walking at different speeds and slopes. J Neurophysiol 122(2):872–887. https://doi.org/10.1152/jn.00167.2019

Dewolf AH, Mesquita RM, De Jaeger D (2022) The effects of an increased step frequency on running economy and injury risk factors during downhill running. Sci Sports 37(5–6):446–453. https://doi.org/10.1016/j.scispo.2021.07.010

Farley CT, González O (1996) Leg stiffness and stride frequency in human running. J Biomech 29(2):181–186. https://doi.org/10.1016/0021-9290(95)00029-1

Ferris DP, Farley CT (1997) Interaction of leg stiffness and surface stiffness during human hopping. J Appl Physiol 82(1):15–22. https://doi.org/10.1152/jappl.1997.82.1.15

Folland JP, Allen SJ, Black MI, Handsaker JC, Forrester SE (2017) Running technique is an important component of running economy and performance. Med Sci Sports Exerc 49(7):1412–1423. https://doi.org/10.1249/MSS.0000000000001245

Gosseye TP, Willems PA, Heglund NC (2010) Biomechanical analysis of running in weightlessness on a treadmill equipped with a subject loading system. Eur J Appl Physiol 110(4):709–728. https://doi.org/10.1007/s00421-010-1549-9

Grasso R, Zago M, Lacquaniti F (2000) Interactions between posture and locomotion: motor patterns in humans walking with bent posture versus erect posture. J Neurophysiol 83(1):288–300. https://doi.org/10.1152/jn.2000.83.1.288

Günther M, Blickhan R (2002) Joint stiffness of the ankle and knee in running. J Biomech 35:1459–1474

He JP, Kram R, McMahon TA (1991) Mechanics of running under simulated low gravity. J Appl Physiol 71(3):863–870. https://doi.org/10.1152/jappl.1991.71.3.863

Ivanenko YP, Cappellini G, Dominici N, Poppele RE, Lacquaniti F (2007) Modular control of limb movements during human locomotion. J Neurosci 27(41):11149–11161. https://doi.org/10.1523/JNEUROSCI.2644-07.2007

Ivanenko YP, d'Avella A, Poppele RE, Lacquaniti F (2008) On the origin of planar covariation of elevation angles during human locomotion. J Neurophysiol 99(4):1890–1898. https://doi.org/10.1152/jn.01308.2007

Lieberman DE, Warrener AG, Wang J, Castillo ER (2015) Effects of stride frequency and foot position at landing on braking force, hip torque, impact peak force and the metabolic cost of running in humans. J Exp Biol 218(21):3406–3414. https://doi.org/10.1242/jeb.125500

Maykranz D, Seyfarth A (2014) Compliant ankle function results in landing-take off asymmetry in legged locomotion. J Theor Biol 6:2

McMahon TA, Cheng GC (1990) The mechanics of running: How does stiffness couple with speed? J Biomech 23:65–78. https://doi.org/10.1016/0021-9290(90)90042-2

Mesquita RM, Dewolf AH, Catavitello G, Osgnach C, di Prampero PE, Willems PA (2020) The bouncing mechanism of running against hindering, or with aiding traction forces: a comparison with running on a slope. Eur J Appl Physiol 120(7):1575–1589. https://doi.org/10.1007/s00421-020-04379-5

Mesquita RM, Dewolf AH, Desimpelaere F, Koussihouede FE, Willems PA, Catavitello G (2021) The bouncing mechanism of running when changing step frequency at a given speed. Comput Methods Biomech Biomed Engin 24(sup1):21–23. https://doi.org/10.1080/10255842.2021.1978758

Miller JR, Van Hooren B, Bishop C, Buckley JD, Willy RW, Fuller JT (2019) A systematic review and meta-analysis of crossover studies comparing physiological, perceptual and performance measures between treadmill and overground running. Sports Med 49(5):763–782. https://doi.org/10.1007/s40279-019-01087-9

Moore IS (2016) Is there an economical running technique? A review of modifiable biomechanical factors affecting running economy. Sports Med 46(6):793–807. https://doi.org/10.1007/s40279-016-0474-4

NuñezLisboa M (2021) Influence of sports background on the bouncing mechanism of running. Sports Biomech 2:1–12

Ogihara N, Oku T, Andrada E, Blickhan R, Nyakatura JA, Fischer MS (2014) Planar covariation of limb elevation angles during bipedal locomotion in common quails (Coturnix coturnix). J Exp Biol 2:2

Ruina A, Bertram JEA, Srinivasan M (2005) A collisional model of the energetic cost of support work qualitatively explains leg sequencing in walking and galloping, pseudo-elastic leg behavior in running and the walk-to-run transition. J Theor Biol 237(2):170–192. https://doi.org/10.1016/j.jtbi.2005.04.004

Schepens B, Willems PA, Cavagna GA (1998) The mechanics of running in children. J Physiol 509(3):927–940

Seyfarth A, Zhao G, Jörntell H (2022) Whole body coordination for self-assistance in locomotion. Front Neurorobot 16:2

Slawinski JS, Billat VL (2004) Difference in mechanical and energy cost between highly, well, and nontrained runners. Med Sci Sports Exerc 36(8):1440–1446. https://doi.org/10.1249/01.MSS.0000135785.68760.96

Van Hooren B, Fuller JT, Buckley JD, Miller JR, Sewell K, Rao G, Barton C, Bishop C, Willy RW (2020) Is motorized treadmill running biomechanically comparable to overground running? A systematic review and meta-analysis of cross-over studies. Sports Med 50(4):785–813. https://doi.org/10.1007/s40279-019-01237-z

van Oeveren BT, de Ruiter CJ, Beek PJ, van Dieën JH (2021) The biomechanics of running and running styles: a synthesis. Sports Biomech. https://doi.org/10.1080/14763141.2021.1873411

Willems PA, Gosseye TP (2013) Does an instrumented treadmill correctly measure the ground reaction forces? Biology Open 2(12):1421–1424. https://doi.org/10.1242/bio.20136379

Willems PA, Cavagna GA, Heglund NC (1995) External, internal and total work in human locomotion. J Exp Biol 198:379–393

Williams KR, Cavanagh PR (1987) Relationship between distance running mechanics, running economy, and performance. J Appl Physiol 63(3):1236–1245. https://doi.org/10.1152/jappl.1987.63.3.1236

Terms and Conditions

Springer Nature journal content, brought to you courtesy of Springer Nature Customer Service Center GmbH (“Springer Nature”).
Springer Nature supports a reasonable amount of sharing of research papers by authors, subscribers and authorised users (“Users”), for small-scale personal, non-commercial use provided that all copyright, trade and service marks and other proprietary notices are maintained. By accessing, sharing, receiving or otherwise using the Springer Nature journal content you agree to these terms of use (“Terms”). For these purposes, Springer Nature considers academic use (by researchers and students) to be non-commercial.
These Terms are supplementary and will apply in addition to any applicable website terms and conditions, a relevant site licence or a personal subscription. These Terms will prevail over any conflict or ambiguity with regards to the relevant terms, a site licence or a personal subscription (to the extent of the conflict or ambiguity only). For Creative Commons-licensed articles, the terms of the Creative Commons license used will apply.
We collect and use personal data to provide access to the Springer Nature journal content. We may also use these personal data internally within ResearchGate and Springer Nature and as agreed share it, in an anonymised way, for purposes of tracking, analysis and reporting. We will not otherwise disclose your personal data outside the ResearchGate or the Springer Nature group of companies unless we have your permission as detailed in the Privacy Policy.
While Users may use the Springer Nature journal content for small scale, personal non-commercial use, it is important to note that Users may not:

1. use such content for the purpose of providing other users with access on a regular or large scale basis or as a means to circumvent access control;
2. use such content where to do so would be considered a criminal or statutory offence in any jurisdiction, or gives rise to civil liability, or is otherwise unlawful;
3. falsely or misleadingly imply or suggest endorsement, approval , sponsorship, or association unless explicitly agreed to by Springer Nature in writing;
4. use bots or other automated methods to access the content or redirect messages
5. override any security feature or exclusionary protocol; or
6. share the content in order to create substitute for Springer Nature products or services or a systematic database of Springer Nature journal content.

In line with the restriction against commercial use, Springer Nature does not permit the creation of a product or service that creates revenue, royalties, rent or income from our content or its inclusion as part of a paid for service or for other commercial gain. Springer Nature journal content cannot be used for inter-library loans and librarians may not upload Springer Nature journal content on a large scale into their, or any other, institutional repository.
These terms of use are reviewed regularly and may be amended at any time. Springer Nature is not obligated to publish any information or content on this website and may remove it or features or functionality at our sole discretion, at any time with or without notice. Springer Nature may revoke this licence to you at any time and remove access to any copies of the Springer Nature journal content which have been saved.
To the fullest extent permitted by law, Springer Nature makes no warranties, representations or guarantees to Users, either express or implied with respect to the Springer nature journal content and all parties disclaim and waive any implied warranties or warranties imposed by law, including merchantability or fitness for any particular purpose.
Please note that these rights do not automatically extend to content, data or other material published by Springer Nature that may be licensed from third parties.
If you would like to use or distribute our Springer Nature journal content to a wider audience or on a regular basis or in any other manner not expressly permitted by these Terms, please contact Springer Nature at

onlineservice@springernature.com